GDCh

Research Articles

Angewandte
Chemie
International Edition
www.angewandte.org

Drug Delivery

Aggregation-Induced Emission Featured Supramolecular Tubisomes for Imaging-Guided Drug Delivery

Jie Yang[+], Xinyang Yu[+], Ji-Inn Song, Qiao Song, Stephen C. L. Hall, Guocan Yu, and Sébastien Perrier*

Abstract: *Polymeric cylinders, a fascinating type of nano-structures with high surface area, internal volume and rigidity, have been exploited as novel drug delivery vehicles over the past decade. However, it's still an open challenge to afford cylindrical nanostructures using polymeric building blocks via traditional self-assembly processes. Herein, we report a hierarchical self-assembly strategy of preparing cylindrical aggregates (tubisomes) from an amphiphilic supramolecular bottlebrush polymer in which a cyclic peptide nanotube is employed as the noncovalent backbone. Additionally, an aggregation-induced emission (AIE) effect was introduced into the tubisomes to endow them with excellent fluorescent properties. Intriguingly, by encapsulating with the anticancer drug doxorubicin (DOX), both the fluorescence of tubisome and DOX can be quenched due to the energy transfer relay (ETR) effect. The release of DOX can induce the interruption of the ETR effect and recover the silenced fluorescence, thereby permitting the in-situ imaging of drug release. The AIE-featured supramolecular tubisomes reported here provide an alternative approach for fabricating cylindrical polymeric nanostructures and holds great potential for imaging-guided drug delivery.*

Introduction

Polymeric nanovehicles have been recognized as an effective solution to manage poor biodistribution and stability of therapeutics.[1] Over the past decades, tremendous efforts have been devoted to understand how their physical and chemical attributes can optimize their therapeutic efficacy.[2] Amongst these attributes, the morphology of polymeric nanovehicles has been identified as an important factor that affects the biological processes.[3] For instance, cylindrical micelles have been reported to show increased in vivo circulation times and different cellular internalization pathways compared to spherical nanoparticles.[4] These structures can be obtained from a range of synthetic polymer chemistry approaches, as well as via microfabrication.[5] For example, bottlebrush polymers are effective cylindrical nanostructures with variable rigidity/flexibility, dimensions, and functionalities.

Inspired by covalent bottlebrush polymers, supramolecular bottlebrush polymers have attracted much attention, in which the polymer backbones are connected by noncovalent bonds, so as to explore a novel approach to afford cylindrical polymeric assemblies.[6] Due to the dynamic nature of noncovalent interactions, polymeric cylinders assembled from supramolecular polymers have tremendous advantages, including stimuli-responsive properties and modular functionalities. Such an approach is based on the self-assembly of cyclic peptides (CPs), a type of ring-shaped flat structures made up of an even number of alternating D- and L-amino acids, which assemble into tubular nanostructures via multiple hydrogen bonding interactions.[7] The self-assembled nanotubes have been shown to be an ideal backbone for the formation of supramolecular bottlebrush polymers.[8] In 2018, we utilized a cyclic peptide as a linker between the hydrophilic and hydrophobic segments of an amphiphilic block copolymer, to drive a hierarchical self-assembly into cylindrical polymeric assemblies (tubisomes) independent of the ratio of the hydrophilic and hydrophobic domains.[9] The tubular self-assembly of cyclic peptide can induce the formation of Janus amphiphilic nanotubes, which present a hydrophobic internal channel and a hydrophilic shell. These tubisomes have been shown to be biocompatible, penetrate cells via endocytosis, and are capable of perforating the lysosome membrane in cells to facilitate the lysosomal escape of drug molecules.[10] In addition, modifications of either cyclic peptides or the conjugated polymers provided the tubisomes with a myriad of functionalities, thus making them versatile drug delivery vehicles.[11]

Toward this end, our studies focus on the design and preparation of functional tubisome nanostructures and their use in drug delivery. In this application, fluorescent labelling is key in order to track their intracellular distribution.[12] We selected tetraphenylethene (TPE), a typical aggregation-induced emission (AIE) fluorophore, as our fluorescent label, since it is well known and has been broadly investigated in an array of applications.[13] In contrast to traditional fluorophores, TPE is not affected by aggregation-caused quenching (ACQ), and it holds promising potential

[*] Dr. J. Yang,[+] J.-I. Song, Dr. Q. Song, Dr. S. C. L. Hall, Prof. S. Perrier
Department of Chemistry, University of Warwick
Coventry CV4 7AL (UK)
E-mail: s.perrier@warwick.ac.uk

Dr. J. Yang[+]
College of Science, Nanjing Forestry University
Nanjing 210037 (P. R. China)

Dr. X. Yu,[+] Dr. G. Yu
Key Laboratory of Bioorganic Phosphorus Chemistry & Chemical Biology, Department of Chemistry, Tsinghua University
Beijing 100084 (P. R. China)
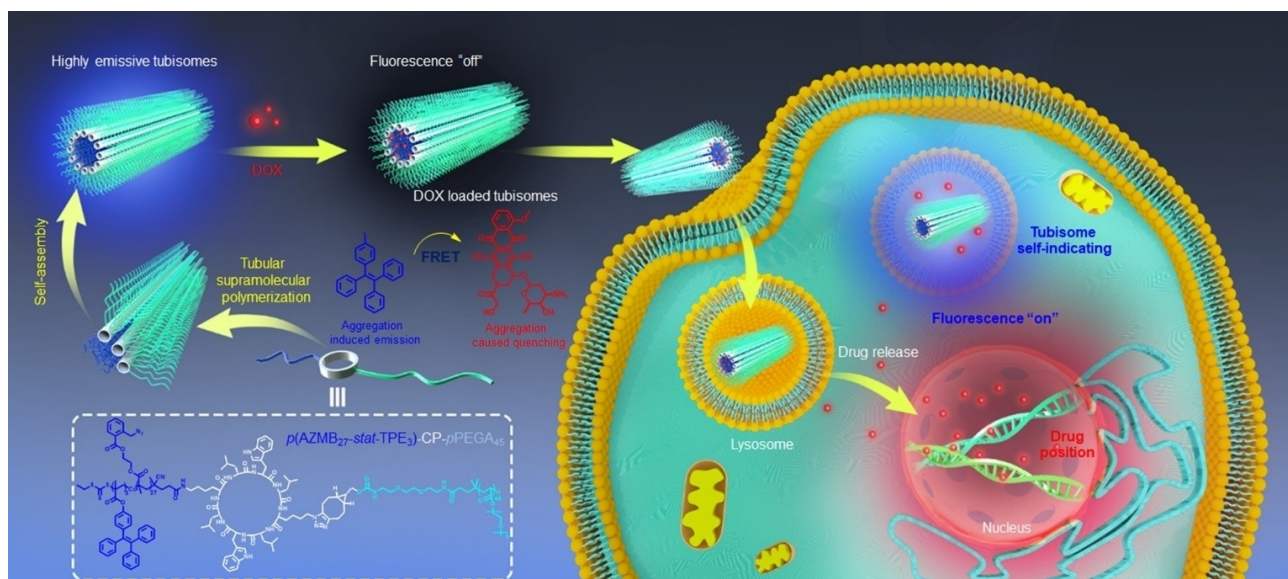
[+] These authors contributed equally to this work.

in simultaneous imaging diagnosis and cancer therapy.[14] Herein, as depicted in Scheme 1, by synergetic combination of aggregation-induced emission effect and cyclic peptide shaped tubular self-assembly, we have constructed a family of multifunctional tubisomes in solution, which shows unique topological structure and excellent fluorescent property. More interestingly, due to the confined hydrophobic core (diameter around 10 nm) of the tubisomes, a Förster Resonance Energy Transfer (FRET) system between the TPE motifs (donor) and the encapsulated anticancer drug DOX (acceptor) was observed, resulting in quenching the fluorescence of TPE.[15] Since DOX shows no fluorescence when encapsulated, due to its inherent ACQ effect, it behaves as a fluorescence "silent" drug when encapsulated in the tubisomes. We exploited the over-expressed glutathione and lower pH in cancer cells to accelerate drug release, which simultaneously result in the interruption of the energy transfer relay and enable the recovery of quenched fluorescence of both TPE (blue) and DOX (red), thereby permitting in situ monitoring of drug release by confocal laser scanning microscopy. Furthermore, in vitro experiments showed that DOX-loaded tubisomes is effective in the inhibition of cancer cells proliferation, indicating their potential as effective cancer drug carriers.

Results and Discussion

In view of the synthesis, reversible addition fragmentation chain transfer (RAFT) polymerization was used to afford both the hydrophobic copolymer p(AZMB$_{27}$-*stat*-TPE$_3$) and hydrophilic polymer poly(PEG acrylate) (pPEGA$_{45}$) with controlled degree of polymerization.[16] An amphiphilic cyclic peptide-polymer conjugate p(AZMB$_{27}$-*stat*-TPE$_3$)-CP-pPEGA$_{45}$ was obtained by orthogonal click reaction and

amidation reaction (synthesis details are given in the Supporting Information).[17] To elucidate the cyclic peptide induced self-assembly, a diblock copolymer pAZMB$_{30}$-b-pPEGA$_{47}$ with similar composition was synthesized as a control. Small angle neutron scattering (SANS) was used to provide an insight into the self-assembly behavior of both cyclic peptide-polymer conjugate and control diblock copolymer in solution. Fitting the scattering data obtained from SANS showed that cylindrical polymer assemblies represent the best model to describe the assembly of cyclic peptide-polymer conjugates (Figure 1a), while the control diblock copolymer assemblies could only be fitted by a spherical polymeric micelle model (Figure 1b), thus indicating the key role of the cyclic peptide in the self-assembly. Of particular note is that the radius of the core of the fitted cylinder is ca. 6.64 nm which is far exceeding the radius of a single cyclic peptide nanotube (around 0.45 nm), thereby suggesting the cyclic peptide-polymer conjugates assemble into tubisomes.[18] We also used transmission electron microscopy (TEM) to assess the morphologies visually. From TEM, we observed rod like nanostructures, with an average length about 115 nm, obtained from a cyclic peptide polymer conjugates solution at 1.0 mg mL^{-1} in water. However, solutions of the control block copolymer show only spherical micelles, thus confirming the SANS data. The distinctly different self-assembled nanostructures confirm that cyclic peptide could be used as an efficient supramolecular polymerisation to control the "modular" self-assembly of block copolymers into cylindrical polymeric assemblies.

Because of the aggregation-induced emission effect of TPE moieties, the self-assembled tubisomes display strong fluorescence in aqueous solution. As shown in Figure 2a,b, cyclic peptide-polymer conjugate exhibited almost no fluorescence in DMSO. In contrast, the emission intensity dramatically increased upon gradually addition of water.

Scheme 1. Left: Chemical structure of p(AZMB$_{27}$-*stat*-TPE$_3$)-CP-pPEGA$_{45}$ and the preparation of DOX-loaded tubisomes. Right: Schematic illustration of the imaging-guided drug delivery.
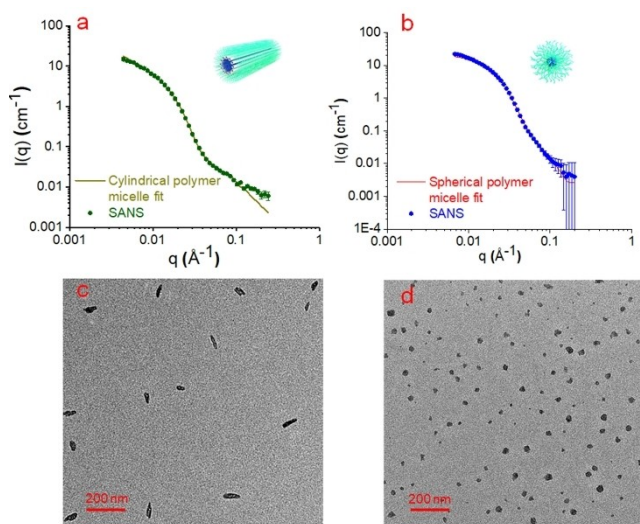
Figure 1. a) SANS plots for the cyclic peptide-polymer conjugate p(AZMB$_{27}$-*stat*-TPE$_3$)-CP-pPEGA$_{45}$. The scattering profiles were best fitted with a cylindrical polymer micelle model (yellow line). b) SANS plots for the control polymer pAZMB$_{30}$-*b*-pPEGA$_{47}$. The scattering profiles were best fitted with a spherical polymer micelle model (red line). TEM images of: c) p(AZMB$_{27}$-*stat*-TPE$_3$)-CP-pPEGA$_{45}$ and d) pAZMB$_{30}$-*b*-pPEGA$_{47}$. The concentration of the prepared samples for TEM is 1.0 mg mL^{-1}.
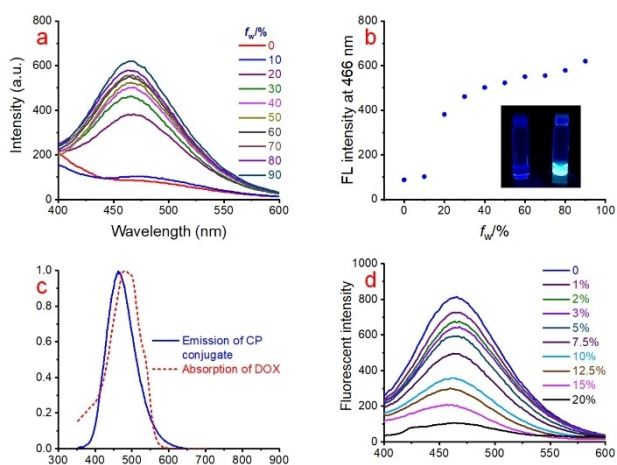

Figure 2. a) Fluorescence spectra of p(AZMB$_{27}$-*stat*-TPE$_3$)-CP-pPEGA$_{45}$ in mixtures of DMSO and water with different f_w values. b) Plot of the emission intensity at 466 nm vs. f_w of the aqueous mixtures. The concentration of p(AZMB$_{27}$-*stat*-TPE$_3$)-CP-pPEGA$_{45}$ was 0.1 mg mL^{-1}. c) Emission spectrum of p(AZMB$_{27}$-*stat*-TPE$_3$)-CP-pPEGA$_{45}$ and absorption spectrum of DOX. d) Fluorescence spectra of tubisomes self-assembled from p(AZMB$_{27}$-*stat*-TPE$_3$)-CP-pPEGA$_{45}$ in the presence of different amounts of DOX.

This effect is explained by the intramolecular rotations of TPE largely restricted in the compact aggregate of the conjugates, thereby enhancing the fluorescence quantum efficiency.[19] Interestingly, the absorption spectrum of doxorubicin, a typical anticancer drug, was observed to overlap with the emission spectrum of the conjugates (Figure 2c). This suggests that we could observe a Förster resonance

energy transfer (FRET) process between DOX and the conjugates, if their spatial distance is appropriate (≈ 10 nm). We confirmed this hypothesis by observing that the fluorescence of TPE is gradually quenched when increasing DOX amount (Figure 2d). Indeed, as DOX is encapsulated within the hydrophobic core of the tubisomes, it brings it close to the TPE moieties (since the radius of the tubisome is around 6.34 nm), thereby enabling the FRET process. Also, DOX self-quenches its fluorescence by the ACQ effect, thus offering a dual-fluorescence-quenched drug carrier.

In order to target the reductive intracellular environment, a unique hydrophobic monomer based on the motif 2-azido-methylbenzoate (AZMB) was designed and polymerized into a hydrophobic segment. This moiety reacts with glutathione to trigger a cascade elimination (Figure 3) and can be easily removed. As a consequence, the hydrophobic segments convert to hydrophilic ones, thereby resulting in the dissociation of self-assembled tubisomes, and the loss of the hydrophobic channel facilitates drug release in cancer cells.[20] The GSH- responsiveness of the AZMB motifs was first investigated by using UV/Vis spectroscopy. In the presence of 10.0 mM GSH, the characteristic absorption
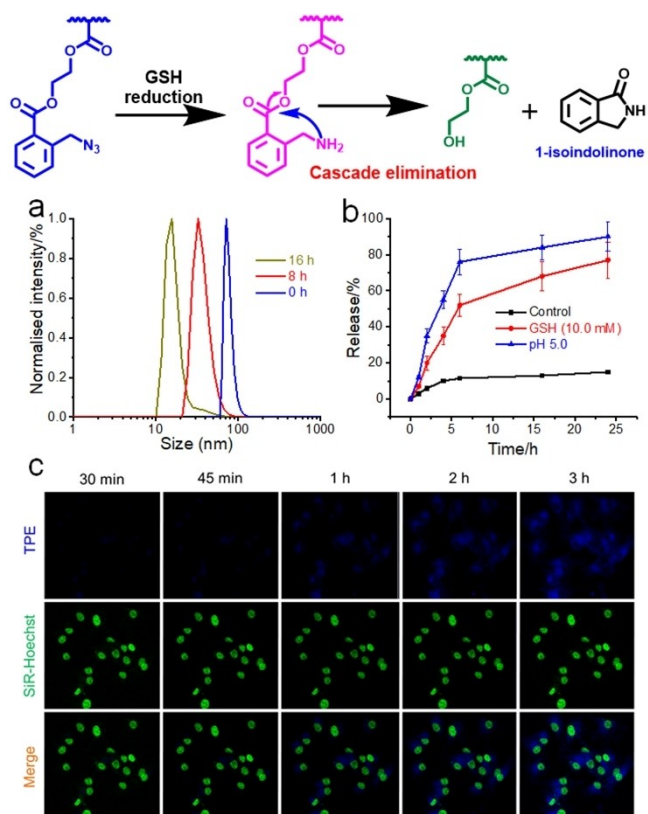

Figure 3. a) Number-weighted size distribution of p(AZMB$_{27}$-*stat*-TPE$_3$)-CP-pPEGA$_{45}$ (1.0 mg mL^{-1}) upon incubation with GSH solution (10 mM). b) Time-dependent drug release behavior of DOX-loaded tubisomes in PBS solution. (black line: pH 7.4; red line: GSH (10.0 mM); blue line: pH 5.0). c) CLSM images of free tubisomes, where the tubsiome was shown in blue, and the SiR-Hoechst was shown in green.

band for the detached 1-isoindolinone at 250 nm was monitored. As shown in Figure S10, the elimination ratio of AZMB increased gradually over a period of 48 h. Similarly, in the proton NMR spectrum of control block copolymer, the characteristic signals for AZMB disappeared completely after 48 h, indicating an efficient elimination reaction in the presence of GSH (Figure S11). TEM images provided another evidence, and showed the controlled and well-defined tubisome structures are transformed into random nano-aggregates after incubation with GSH (Figure S12). Additionally, a significant size decrease for the aggregates is observed from DLS which is in good agreement with TEM images (Figure 3a).

The toxicity of $p(AZMB_{27}\text{-}stat\text{-}TPE_3)\text{-}CP\text{-}pPEGA_{45}$ was evaluated on different cell lines. As indicated in Figure S13, even at the concentration of $p(AZMB_{27}\text{-}stat\text{-}TPE_3)\text{-}CP\text{-}pPEGA_{45}$ of $200\ \mu g\,mL^{-1}$, no obvious cytotoxicity was observed to any of the treated cell lines, indicating excellent biocompatibility of the tubisomes. Moreover, the internalization behavior of a control (empty) tubisomes was studied by real-time confocal laser scanning microscopy (CLSM). The fluorescence (blue color) from tubisomes was clearly observed after 1 h incubation, and did not overlap with the green fluorescence of SiR-Hoechst (Figure 3c). Furthermore, the blue fluorescence overlapped with the red fluorescence of LysoTracker (Figure S17), which provides direct evidence that the tubisomes are located in lysosomes and not in the nucleus. Spatiotemporal distribution of tubisomes was studied by means of the increments of tubisome fluorescence intensity in lysosome as a function of incubation time. As shown in Figure S16, the TPE fluorescence intensity enhanced gradually in lysosome upon increasing incubation time, suggesting successfully internalization of tubisomes through a time-dependent manner.

Considering the hydrophobic circumstance of the core of self-assembled nanostructures, tubisomes could be used to load hydrophobic drugs. Doxorubicin was successfully encapsulated into tubisomes with a drug loading content of 12.1 wt.%. Furthermore, TEM (Figure S20) and DLS (Figure S21) were conducted to study the morphology changes of the tubisomes after DOX loading. Compared to free tubisomes, the average size of DOX-loaded tubisomes increased slightly, indicating the negligible influence of DOX loading on the morphology and size of the tubisomes. The release of DOX was then studied by GSH-triggered disassembly of the tubisomes. As shown in Figure 3b, at neutral pH without GSH, only 16% of encapsulated DOX was released within 24 h, suggesting the excellent stability of the tubisome carriers under physiological conditions. As expected, an accelerated release was observed in the presence of GSH, with a release increased to 76%. Additionally, due to the acidic intracellular environment, the encapsulated DOX is protonated, thereby accelerating its escape from tubisomes. As shown in Figure 3b, at pH 5.0, 90% of DOX was released from DOX-loaded tubisomes after 24 h which is much higher than that at neutral pH, indicating lower pH can speed up the DOX release.

It is worth noting that the fluorescence of DOX and TPE is recovered when DOX is released due to the

interruption of the ETR effect, which means in situ monitoring of the drug release is possible via tracking the spatiotemporal transition of the different fluorescent wavelengths. To prove this assumption, the internalization and distribution behavior of the empty tubisomes, free DOX and DOX-loaded tubisomes were followed by confocal laser scanning microscopy (CLSM). Figure 4 shows that the fluorescence (blue color) from tubisomes is observed in lysosomes and does not overlap with the green color from SiR-Hoechst, which indicates that tubisomes are located in lysosomes and do not penetrate the nucleus. As we expected, the fluorescence of free DOX (red color) mainly located in the nucleus where it interacts with the DNA. The CLSM images of DOX-loaded tubisomes were taken at different incubation timepoints. As indicated in Figure 4, distinct TPE and DOX fluorescence were detected for the cells after 2 h incubation with tubisome/DOX. Noteworthy, the fluorescent intensity gradually enhanced with incubation time, indicating a time-dependent drug release manner from tubisomes. The blue fluorescence of TPE was observed in the lysosomes, in the same location compared with free tubisomes. Besides, there is no TPE signals detected in the nucleus, suggesting that tubisomes just acts as delivery vehicles. As for the red fluorescence channel, DOX was mainly located in lysosomes within 2 h incubation, and colocalized with the fluorescence of TPE. In 8 h incubation, DOX was observed in both the lysosomes and nucleus, indicating that DOX escaped from lysosomes and entered into the cell nucleus. By extending incubation time to 12 h, the fluorescence intensity of both TPE and DOX increased, and most DOX distributed in nucleus. The increments of DOX fluorescence intensity as a function of incubation time in both lysosome and nucleus were evaluated. As shown in Figure S19, the fluorescence of DOX increased gradually upon increasing incubation time. Noteworthy, at nearly 4 h
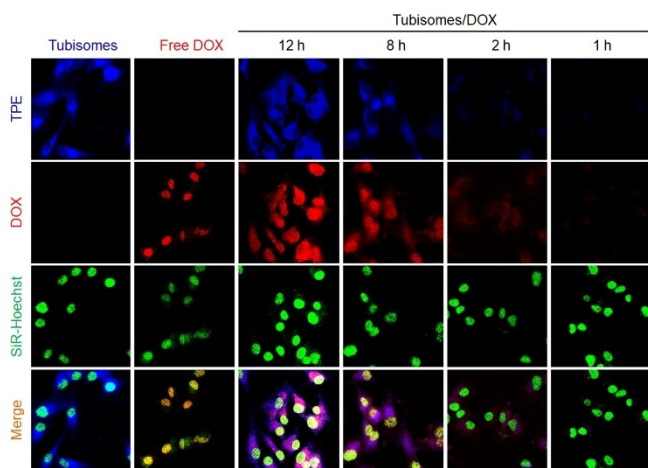

Figure 4. Spatial distributions of tubisomes, free DOX and DOX-loaded tubisomes in MDA-MB-231 cells. CLSM images of self-indicating tubisomes, free DOX and DOX-loaded tubisomes, and nucleus, indicated by SiR-Hoechst. The MDA-MB-231 cells were incubating with tubisomes (40 μM) and DOX (4 μM) for 12 h, with DOX-loaded tubisomes (40 μM) for 1 h, 2 h, 8 h, 12 h. Scale bars are 30 μm.

timepoint, the fluorescence intensity of DOX in the nucleus is higher than that in the lysosomes, indicating that DOX was released in lysosome and gradually entered in the nucleus and perform its toxicity. By tracking the spatiotemporal location of the different colours, we hypothesized that tubisomes deliver the anticancer drug DOX into cells and localise in lysosomes, where DOX is released due to the reductive and acidic environments. The released DOX escapes from lysosomes and accumulates in the nucleus, while tubisomes still stay in lysosomes.

In vitro cytotoxicity of DOX-loaded tubisomes was evaluated by 2,3-bis[2-methoxy-4-nitro-5-sulfophenyl]-2H-tetrazolium-5-carboxanilide (XTT) assay, with blank tubisomes and free DOX used as control on human breast cancer cells. As indicated in Figure S14, decreased cell viability was observed upon increasing the concentration of DOX. The half-maximal inhibitory concentration (IC_{50}) of free DOX was measured at $7.4\,\mu g\,mL^{-1}$, while the IC_{50} of DOX-loaded tubisomes was estimated to be $6.3\,\mu g\,mL^{-1}$, which is slightly higher than the value obtained for free DOX, showing that tubisome are efficient drug delivery vehicles.

Conclusion

In conclusion, we have developed a novel drug delivery vehicle based on aggregation-induced emission and cyclic peptide shaped tubular self-assembly, which shows unique topological structure and excellent fluorescent properties. The amphiphilic cyclic peptide polymer conjugate assembled into cylindrical structures, which provide an efficient strategy to obtain non-spherical nanostructures. Furthermore, the AIE effect provides the tubisomes with inherent fluorescence and make them easily trackable inside the cells. The obtained tubisomes show excellent biocompatibility and were used as carriers for the anticancer drug DOX. Interestingly, we observed that the fluorescence of both TPE and DOX can be quenched due to the ETR effect mediated by FRET and ACQ effects. Nevertheless, in the presence of over-expressed glutathione and lower pH inside cancer cells, DOX is released from the tubisomes, which results in the interruption of the ETR effect between TPE and DOX, thereby permitting the recovery of the fluorescence from both TPE and DOX. Confocal laser scanning microscopy enables us to locate where the drug is released and its site of action. We established that tubisomes are transported into lysosomes, where DOX is released. The released DOX then escaped from the lysosomes and migrates to the cell nucleus while tubisomes remained in the lysosomes. Overall, we found that the DOX-loaded tubisomes are highly efficient in inhibiting the proliferation of cancer cells. In conclusion, this work provides an efficient method to prepare cylindrical polymeric nanostructures and a powerful drug delivery method that can track the intracellular location of the delivery vehicles and the drug release, with great potential in cancer therapy.

Conflict of Interest

The authors declare no conflict of interest.

Data Availability Statement

The data that support the findings of this study are available from the corresponding author upon reasonable request.

[1] a) J. Kost, R. Langer, *Adv. Drug Delivery Rev.* **2001**, *46*, 125–148; b) N. Kamaly, B. Yameen, J. Wu, O. C. Farokhzad, *Chem. Rev.* **2016**, *116*, 2602–2663; c) S. Pottanam Chali, B. J. Ravoo, *Angew. Chem. Int. Ed.* **2020**, *59*, 2962–2972; *Angew. Chem.* **2020**, *132*, 2982–2993; d) K. Yang, G. Yu, R. Tian, Z. Zhou, H. Deng, L. Li, Z. Yang, G. Zhang, D. Liu, J. Wei, L. Yue, R. Wang, X. Chen, *Adv. Funct. Mater.* **2021**, *31*, 2008078.

[2] a) A. K. Bajpai, S. K. Shukla, S. Bhanu, S. Kankane, *Prog. Polym. Sci.* **2008**, *33*, 1088–1118; b) X. Fu, L. Hosta-Rigau, R. Chandrawati, J. Cui, *Chem* **2018**, *4*, 2084–2107; c) K. Yang, G. Yu, Z. Yang, L. Yue, X. Zhang, C. Sun, J. Wei, L. Rao, X. Chen, R. Wang, *Angew. Chem. Int. Ed.* **2021**, *60*, 17570–17578.

[3] a) S. Venkataraman, J. L. Hedrick, Z. Y. Ong, C. Yang, P. L. R. Ee, P. T. Hammond, Y. Y. Yang, *Adv. Drug Delivery Rev.* **2011**, *63*, 1228–1246; b) N. P. Truong, M. R. Whittaker, C. W. Mak, T. P. Davis, *Expert Opin. Drug Delivery* **2015**, *12*, 129–142.

[4] a) Y. Geng, P. Dalhaimer, S. Cai, R. Tsai, M. Tewari, T. Minko, D. E. Discher, *Nat. Nanotechnol.* **2007**, *2*, 249–255; b) J. Zhao, H. Lu, P. Xiao, M. H. Stenzel, *ACS Appl. Mater. Interfaces* **2016**, *8*, 16622–16630; c) J. A. Foster, S. Varlas, B. Couturaud Z Coe, R. K. O'Reilly, *J. Am. Chem. Soc.* **2019**, *141*, 2742–2753.

[5] a) A. Blanazs, S. P. Armes, A. J. Ryan, *Macromol. Rapid Commun.* **2009**, *30*, 267–277; b) B. Charleux, G. Delaittre, J. Rieger, F. D'Agosto, *Macromolecules* **2012**, *45*, 6753–6765; c) J. B. Gilroy, T. Gadt, G. R. Whittell, L. Chabanne, J. M. Mitchels, R. M. Richardson, M. A. Winnik, I. Manners, *Nat. Chem.* **2010**, *2*, 566–570; d) S. S. Sheiko, B. S. Sumerlin, K. Matyjaszewski, *Prog. Polym. Sci.* **2008**, *33*, 759–785.

[6] a) J. Roosma, T. Mes, P. Leclere, A. R. Palmans, E. W. Meijer, *J. Am. Chem. Soc.* **2008**, *130*, 1120–1121; b) S. Catrouillet, C. Fonteneau, L. Bouteiller, N. Delorme, E. Nicol, T. Nicolai, S. Pensec, O. Colombani, *Macromolecules* **2013**, *46*, 7911–7919; c) V. Saez Talens, P. Englebienne, T. T. Trinh, W. E. M. Noteborn, I. K. Voets, R. E. Kieltyka, *Angew. Chem. Int. Ed.* **2015**,

Angew. Chem. Int. Ed. **2022**, *61*, e202115208 (5 of 6)

© 2021 Wiley-VCH GmbH

54, 10502–10506; *Angew. Chem.* **2015**, *127*, 10648–10652; d) D. Spitzer, L. L. Rodrigues, D. Straßburger, M. Mezger, P. Besenius, *Angew. Chem. Int. Ed.* **2017**, *56*, 15461–15465; *Angew. Chem.* **2017**, *129*, 15664–15669.

[7] a) M. R. Ghadiri, J. R. Granja, R. A. Milligan, D. E. McRee, N. Khazanovich, *Nature* **1993**, *366*, 324–327; b) M. R. Ghadiri, J. R. Granja, L. K. Bühler, *Nature* **1994**, *369*, 301–304; c) S. Fernandez-Lopez, H. S. Kim, E. C. Choi, M. Delgado, J. R. Granja, A. Khasanov, K. Kraehenbuehl, G. Long, D. A. Weinberger, K. M. Wilcoxen, M. R. Ghadiri, *Nature* **2001**, *412*, 452–455.

[8] a) M. Danial, C. M. N. Tran, K. A. Jolliffe, S. Perrier, *J. Am. Chem. Soc.* **2014**, *136*, 8018–8026; b) S. C. Larnaudie, J. C. Brendel, K. A. Jolliffe, S. Perrier, *ACS Macro Lett.* **2017**, *6*, 1347–1351; c) J. Y. Rho, J. C. Brendel, L. R. MacFarlane, E. D. Mansfield, R. Peltier, S. Rogers, M. Hartlieb, S. Perrier, *Adv. Funct. Mater.* **2018**, *28*, 1704569–1704579; d) Q. Song, J. Yang, J. Y. Rho, S. Perrier, *Chem. Commun.* **2019**, *55*, 5291–5294; e) Q. Song, S. Goia, J. Yang, S. C. L. Hall, M. Staniforth, V. G. Stavros, S. Perrier, *J. Am. Chem. Soc.* **2021**, *143*, 382–389.

[9] J. C. Brendel, S. Catrouillet, J. Sanchis, K. A. Jolliffe, S. Perrier, *Polym. Chem.* **2019**, *10*, 2616–2625.

[10] J. C. Brendel, J. Sanchis, S. Catrouillet, E. Czuba, M. Z. Chen, B. M. Long, C. Nowell, A. Johnston, K. A. Jolliffe, S. Perrier, *Angew. Chem. Int. Ed.* **2018**, *57*, 16678–16682; *Angew. Chem.* **2018**, *130*, 16920–16924.

[11] J. Yang, J.-I. Song, Q. Song, J. Y. Rho, E. D. H. Mansfield, S. C. L. Hall, M. Sambrook, F. Huang, S. Perrier, *Angew. Chem. Int. Ed.* **2020**, *59*, 8860–8863; *Angew. Chem.* **2020**, *132*, 8945–8948.

[12] a) R. Weissleder, M. J. Pittet, *Nature* **2008**, *452*, 580–589; b) J. R. W. Conway, N. O. Carragher, P. Timpson, *Nat. Rev. Cancer* **2014**, *14*, 314–328; c) M. Gao, F. Yu, C. Lv, J. Choo, L. Chen, *Chem. Soc. Rev.* **2017**, *46*, 2237–2271.

[13] a) Y. Hong, J. W. Y. Lam, B. Z. Tang, *Chem. Soc. Rev.* **2011**, *40*, 5361–5388; b) J. Mei, N. L. C. Leung, R. T. K. Kowk, J. W. Y. Lam, B. Z. Tang, *Chem. Rev.* **2015**, *115*, 11718–11940.

[14] a) M. Li, Y. Gao, Y. Yuan, Y. Wu, Z. Song, B. Z. Tang, B. Liu, Q. C. Zheng, *ACS Nano* **2017**, *11*, 3922–3932; b) G. Yu, M. Zhang, M. L. Saha, Z. Mao, J. Chen, Y. Yao, Z. Zhou, Y. Liu, C. Gao, F. Huang, X. Chen, P. J. Stang, *J. Am. Chem. Soc.* **2017**, *139*, 15940–15949.

[15] a) X. Xue, Y. Zhao, L. Dai, X. Zhang, X. Hao, C. Zhang, S. Huo, J. Liu, C. Liu, A. Kumar, W.-Q. Chen, G. Zou, X.-J. Liang, *Adv. Mater.* **2014**, *26*, 712–717; b) G. Yu, R. Zhao, D. Wu, F. Zhang, L. Shao, J. Zhou, J. Yang, G. Tang, X. Chen, F. Huang, *Polym. Chem.* **2016**, *7*, 6178–6188; c) D. Wu, Y. Li, J. Yang, J. Shen, J. Zhou, Q. Hu, G. Yu, G. Tang, X. Chen, *ACS Appl. Mater. Interfaces* **2017**, *9*, 44392–44401.

[16] a) S. Perrier, P. Takolpuckdee, *J. Polym. Sci. Part A* **2005**, *43*, 5347–5393; b) W. A. Braunecker, K. Matyjaszewski, *Prog. Polym. Sci.* **2007**, *32*, 93–146.

[17] a) M. Danial, C. My-Nhi Tran, P. G. Young, S. Perrier, K. A. Jolliffe, *Nat. Commun.* **2013**, *4*, 2780–2792; b) D. M. Beal, L. H. Jones, *Angew. Chem. Int. Ed.* **2012**, *51*, 6320–6326; *Angew. Chem.* **2012**, *124*, 6426–6432.

[18] M. R. Ghadiri, K. Kobayashi, J. R. Granja, R. K. Chadha, D. E. McRee, *Angew. Chem. Int. Ed. Engl.* **1995**, *34*, 93–95; *Angew. Chem.* **1995**, *107*, 76–78.

[19] Y. Hong, J. W. Y. Lam, B. Z. Tang, *Chem. Commun.* **2009**, 4332–4353.

[20] a) T. Wada, A. Ohkubo, A. Mochizuki, S. Sekine, *Tetrahedron Lett.* **2001**, *42*, 1069–1072; b) Q. Yan, W. Sang, *Chem. Sci.* **2016**, *7*, 2100–2105.